Faraday Discussions

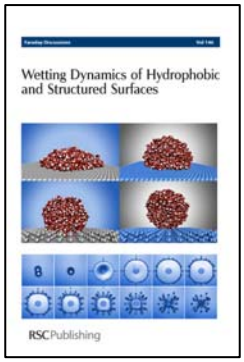

This paper is published as part of Faraday Discussions volume 146: Wetting Dynamics of Hydrophobic and Structured Surfaces

Introductory Lecture

Papers

Discussion

Papers

Molecular dynamics simulations of urea–water binary droplets on flat and pillared hydrophobic surfaces
Takahiro Koishi, Kenji Yasuoka, Xiao Cheng Zeng and Shigenori Fujikawa, *Faraday Discuss.*, 2010
DOI: 10.1039/b926919c

Discussion

General discussion
Faraday Discuss., 2010
DOI: 10.1039/c005416j

Papers

First- and second-order wetting transitions at liquid–vapor interfaces
K. Koga, J. O. Indekeu and B. Widom, *Faraday Discuss.*, 2010
DOI: 10.1039/b925671g

Hierarchical surfaces: an *in situ* investigation into nano and micro scale wettability
Alex H. F. Wu, K. L. Cho, Irving I. Liaw, Grainne Moran, Nigel Kirby and Robert N. Lamb, *Faraday Discuss.*, 2010
DOI: 10.1039/b927136h

An experimental study of interactions between droplets and a nonwetting microfluidic capillary
Geoff R. Willmott, Chiara Neto and Shaun C. Hendy, *Faraday Discuss.*, 2010
DOI: 10.1039/b925588e

Hydrophobic interactions in model enclosures from small to large length scales: non-additivity in explicit and implicit solvent models
Lingle Wang, Richard A. Friesner and B. J. Berne, *Faraday Discuss.*, 2010
DOI: 10.1039/b925521b

Water reorientation, hydrogen-bond dynamics and 2D-IR spectroscopy next to an extended hydrophobic surface
Guillaume Stirnemann, Peter J. Rossky, James T. Hynes and Damien Laage, *Faraday Discuss.*, 2010
DOI: 10.1039/b925673c

Discussion

General discussion
Faraday Discuss., 2010
DOI: 10.1039/c005417h

Papers

The search for the hydrophobic force law
Malte U. Hammer, Travers H. Anderson, Aviel Chaimovich, M. Scott Shell and Jacob Israelachvili, *Faraday Discuss.*, 2010
DOI: 10.1039/b926184b

The effect of counterions on surfactant-hydrophobized surfaces
Gilad Silbert, Jacob Klein and Susan Perkin, *Faraday Discuss.*, 2010
DOI: 10.1039/b925569a

Hydrophobic forces in the wetting films of water formed on xanthate-coated gold surfaces
Lei Pan and Roe-Hoan Yoon, *Faraday Discuss.*, 2010
DOI: 10.1039/b926937a

Interfacial thermodynamics of confined water near molecularly rough surfaces
Jeetain Mittal and Gerhard Hummer, *Faraday Discuss.*, 2010
DOI: 10.1039/b925913a

Mapping hydrophobicity at the nanoscale: Applications to heterogeneous surfaces and proteins
Hari Acharya, Srivathsan Vembanur, Sumanth N. Jamadagni and Shekhar Garde, *Faraday Discuss.*, 2010
DOI: 10.1039/b927019a

Discussion

General discussion
Faraday Discuss., 2010
DOI: 10.1039/c005418f

Concluding remarks

Concluding remarks for FD 146: Answers and questions
Frank H. Stillinger, *Faraday Discuss.*, 2010
DOI: 10.1039/c005398h

The influence of molecular-scale roughness on the surface spreading of an aqueous nanodrop

Christopher D. Daub,* Jihang Wang, Shobhit Kudesia, Dusan Bratko* and Alenka Luzar*

Received 22nd December 2009, Accepted 26th January 2010
DOI: 10.1039/b927061m

We examine the effect of nanoscale roughness on spreading and surface mobility of water nanodroplets. Using molecular dynamics, we consider model surfaces with sub-nanoscale asperities at varied surface coverage and with different distribution patterns. We test materials that are hydrophobic, and those that are hydrophilic in the absence of surface corrugations. Interestingly, on *both* types of surfaces, the introduction of surface asperities gives rise to a *sharp increase* in the apparent contact angle. The Cassie–Baxter equation is obeyed approximately on hydrophobic substrates, however, the *increase* in the contact angle on a hydrophilic surface differs qualitatively from the behavior on macroscopically rough surfaces described by the Wenzel equation. On the hydrophobic substrate, the superhydrophobic state with the maximal contact angle of 180 degrees is reached when the asperity coverage falls below 25%, suggesting that superhydrophobicity can also be achieved by the nanoscale roughness of a macroscopically smooth material. We further examine the effect of surface roughness on droplet mobility on the substrate. The apparent diffusion constant shows a dramatic slow down of the nanodroplet translation even for asperity coverage in the range of 1% for a hydrophilic surface, while droplets on corrugated hydrophobic surfaces retain the ability to flow around the asperities. In contrast, for smooth surfaces we find that the drop mobility on the hydrophilic surface *exceeds* that on the hydrophobic one.

I. Introduction

Two models are often applied to provide practical estimates for contact angles of macroscopic sessile liquid drops on corrugated surfaces. When the liquid in a drop can wet the surface, the Wenzel picture[1] predicts that, on the corrugated surface the added interfacial area causes the contact angle to differ from the Young angle on the smooth surface θ_Y:

$$\cos\theta_c = R\cos\theta_Y \tag{1}$$

Here, parameter R is the ratio of the surface area on the corrugated surface to the projected area on the smooth surface. When the surface is chemically or geometrically heterogeneous, the model of Cassie and Baxter[2] assumes that the cosine of the contact angle θ_c of the drop on a mixed surface can be approximated by a linear combination of the cosines of contact angles of the components of the surface:

Department of Chemistry, Virginia Commonwealth University, Richmond, VA, USA. E-mail: cdaub@vcu.edu; dnb@berkeley.edu; aluzar@vcu.edu

$$\cos\theta_c = \sum_i f_i R_i \cos\theta_{i,Y}$$

where f_i, $\theta_{i,Y}$ and R_i are the projected surface fractions, contact angles, and roughness parameters for homogeneous surfaces made up of each component i of the surface. Useful estimates of cos θ_c are expected presuming the average properties of the substrate surface are representative of those of the surface under the three-phase contact line.[3] The original Cassie–Baxter equation considered the scenario where one of the surface components was air, or vapor, trapped between chemically homogeneous surface asperities.[2] Contact angle on smooth air pocket surface was assumed to be 180°. The second component comprised wetted asperity tips with contact angle θ_a and roughness (the ratio of wetted area and its projection on the surface plane) $R_a \sim 1$. Assuming $R_a \sim 1$ ($\theta_a = \theta_{a,Y}$), the contact angle can be given by a simplified expression,

$$\cos\theta_c = f_a(\cos\theta_a + 1) - 1 \quad (3)$$

where f_a and $(1 - f_a)$ are the surface fractions of the surface covered by exposed asperity tips and air, respectively. Equation (2) can also be applied to describe a partially wetted surface when R_a exceeds unity but does not depend on f_a, provided R_a is already absorbed in cos θ_a according to Eq. (1).

Traditionally the two regimes described by Eqs. (1) and (3) have been thought to apply to different surface interactions between liquid and solid. For lyophobic interactions, the surface does not wet and the Cassie–Baxter equation, Eq. (3) should predict θ_c, while for lyophilic interactions the Wenzel equation, Eq. (1) should apply.

Both of these models were developed to describe surfaces with macro- or mesoscopic corrugations, and even in this regime the details of the geometry of surface corrugations can be important, with the interpretation of these details also leading to some controversy. For example, whether the patches of each component lie below the bulk of the drop or under the contact line could be important.[4–8] Another effect not accounted for by these equations is the possibility of kinetic barriers, which may force the drop to remain in a metastable state.[9] At the nanoscale where atomic and molecular details become significant, we might expect new influences on the microscopic analogue of the contact angle.[10,11] Clearly, the concepts of surface tension and contact angle are not rigorous when drop dimensions and the length scale of surface texture become comparable to the range of molecular interactions. Nonetheless, for nanodrops exceeding a few tens of Angstroms (above Tolman length in water) the contact angle has been generally regarded as a useful measure of surface wettability in this regime.[12] A few theoretical studies of surfaces with nano-sized roughness have been reported, both by simulation,[13–15] and with analytical work[16,17] but for the most part these studies have focused on corrugated surfaces where the length scale of the roughness is sufficiently large to allow water molecules to coat the rough surface, if this is energetically favorable. Our study focuses on nanoscale surface roughness over a wide range of surface-pattern length scales, so that we can explore the transition between surfaces with low asperity coverage to high-coverage regimes where the space between asperities becomes too tight for hydrogen-bonded water molecules to penetrate into the rough surface. We have come across one study of water droplets on randomly roughened hydrophilic and hydrophobic surfaces,[14] which makes the important point that the typical molecule–molecule separation is much larger than the atomic separation in a typical substrate (see for example Fig. 24 in Ref. 14), and hence the Cassie-like state may be preferred in cases where the length scale of the surface roughness is very small. Other than this, however, the transition from nanoscopic to mesoscopic roughness has not been much addressed.

To study the transition between surfaces with nano- and mesocopic inter-asperity spacings, we have completed simulations of sessile water drops on a variety of atomically corrugated surfaces, constructed by adding partially occupied atomic layers on

top of a regular, (111) graphite-like model surface. For high fractions of these additional atoms, our findings are in qualitative agreement with the Cassie–Baxter equation, but deviate noticeably, with the contact angles being larger than those predicted by the equation. As the coverage lowers, the water drop can penetrate down into these partial layers, and the contact angle lowers. However, we never observe Wenzel behavior, as the contact angle is always *higher* than that on the original, molecularly smooth surface.

We also report interesting data on the lateral mobility of water drops on corrugated surfaces. Koishi and coworkers have studied the vertical mobility of water drops on surfaces with very deep corrugations,[13] but not lateral motions. Lundgren and coworkers have demonstrated that water molecules on mixed surfaces will flow to the hydrophilic regions,[15] but have not quantified these observations. In this study we have quantified the motion of water nanodrops on corrugated surfaces by computing the diffusion constants of the water nanodrops on nano-corrugated surfaces. These calculations reveal that water droplets become "pinned" on hydrophilic surfaces with only a few asperities under each water nanodrop, while droplets on corrugated hydrophobic surfaces retain the ability to flow around the asperities. In contrast, for smooth surfaces we find that the nanodrop motion due to thermal fluctuations is faster on the hydrophilic surface than on the hydrophobic one.

II. Models and methods

We simulate sessile water drops, consisting of 2000 molecules of SPC/E[18] water. Additional simulations with 4000 molecules showed no significant finite-size effects. We used a recent version of the LAMMPS code[19] to do classical molecular dynamics (MD) simulations in the NVT ensemble, using a Nosé-Hoover thermostat to maintain a temperature of 300 K. The surfaces are modeled on the (111) face of graphite, as we[20] and others[21] have done in previous work on sessile water drops. The simulation box is a rectangular prism measuring $117.9 \times 119.1 \times 200$ Å^3, and periodic boundary conditions are implemented throughout by using Ewald sums. This procedure removes the need to use a cut-off for intermolecular potentials without dramatically increasing the computation cost. The contact angles are also computed in the same fashion as in our previous work,[20] by modeling the edge of the drop as a circular section and extrapolating down to the surface of the substrate.

Clearly, for nanodroplets the range of intermolecular potentials is not negligible compared to other characteristic length scales, notably the droplet size. This renders the choice of the drop/substrate contact plane, the position of the three-phase coexistence line, and the resulting value of the contact angle itself slightly arbitrary. Specifically, the droplet contour that determines the contact angle must be extrapolated from a few water layers height down to the contact plane as described in detail in our previous work[20] and by others.[21,22] To validate this established simulation procedure for contact angle calculations, we have performed direct comparisons between simulated contact angles on smooth surfaces with those calculated from wetting surface free energies[23,24] for laterally infinite surfaces,[25] determined by applying the pressure tensor technique[26] on identical but fully wetted surfaces. These *thermodynamic* calculations do not depend on any assumption regarding the precise location of the interface, or on a specific technique for contact angle sampling from the droplet shape. Despite small finite-size effects[21] reported in previous nanodrop calculations, a general agreement between the average contact angles of nanodroplets and thermodynamic calculations of wetting surface free energies, $\Delta\gamma = \gamma_{sl} - \gamma_{sv} \cong \gamma_{lv}\cos\theta_c$, was nonetheless established. Here $\gamma_{\alpha\beta}$ are the interfacial free energies between solid (s), liquid (l) or vapor (v) phases. Both types of calculations pertain to equilibrium situations, which are by definition unable to confirm the presence or lack of hysteresis effects consistently observed in macroscopic experiments.

By tuning the Lennard-Jones interaction between the surface atoms and the oxygen atoms of water molecules in the drop, behaviors ranging from extremely

Table 1 Lennard-Jones parameters and contact angles θ_c for atomically smooth surfaces. The surface lattice is that of the (111) face of graphite. Contact angles are determined from several 400 ps MD simulations, and quoted errors are one standard deviation in the mean

σ_{CO}/Å	ε_{CO}/kJ mol^{-1}	θ_c/°
3.190	0.50	59 ± 1
3.190	0.25	118 ± 1
3.230	0.165	139 ± 1
3.190	0.117	153 ± 1

hydrophobic to extremely hydrophilic may be captured. In Table 1 we show all of the examples of Lennard-Jones parameters and observed θ_c on atomically smooth, homogeneous surfaces that we have studied in this work. The first two models are the same as cases 19 and 17, respectively, from Werder *et al.*[21] Our contact angles are somewhat lower due to the omission of a pair-potential cut-off applied in Ref. 21.

Systems were equilibrated for at least 400 ps before contact angles were computed, with equilibration extended up to 1.2 ns for cases where additional time was required for contact angles to stabilize. Each determination of the contact angle was derived from one 400 ps trajectory, and was repeated several times until sufficient data to report a reasonable mean contact angle was obtained.

We construct nanoscale corrugated surfaces by addition of carbon atoms into two partially occupied layers on top of a regular, two-layer (111) graphite surface. These atoms are located at the same positions they would be located if additional, full atomic layers were added. Examples of the surfaces we have used are depicted in a simplified representation in Fig. 1, along with representative snapshots from some of the simulations. Identical corrugation topologies, illustrated in the top section of Fig. 1 were considered for both the hydrophobic and hydrophilic materials. Since the droplets on corrugated hydrophobic surfaces consistently displayed Cassie type behavior, a single graph (graph 3 in the bottom row) corresponds to this type of the surface and the remaining snapshots illustrate droplet spreading on model hydrophilic substrates over the whole range of asperity coverage.

III. Results and discussion

Contact angles

In Fig. 1 we display some snapshots of simulated water drops on varied corrugated surfaces. In Fig. 2 we show the contact angles obtained on corrugated surfaces. We have used two different models for the substrate atoms in our study, one hydrophilic (first row in Table 1) and one hydrophobic (second row in Table 1). At high coverage, we observe that θ_c rises as the density of additional atoms reduces, in accordance with the predictions of the Cassie–Baxter equation. However, our observed contact angles deviate from the Cassie–Baxter equation, being more hydrophobic. In fact, in the case of hydrophobic water–graphite interactions, below an areal coverage of 1/6 (shown in Fig. 1) we start to observe superhydrophobic[9,27] behavior. Here, the apparent contact angle θ_c reaches or even exceeds 180°, as the droplet contour, hanging over asperities, no longer intersects the asperity height. To ensure that this discrepancy is not a by-product of our choice of surface construction, we have verified that when we replace the vacancies by extremely hydrophobic atoms (third row in Table 1), the Cassie–Baxter equation is an excellent predictor of θ_c.

In nature, superhydrophobicity often results from a two-scale roughness, the macroscopic roughness combined with finer roughness at the μm scale. Our models confirm that superhydrophobicity can also be achieved by nanoscale roughening of a macroscopically smooth material.

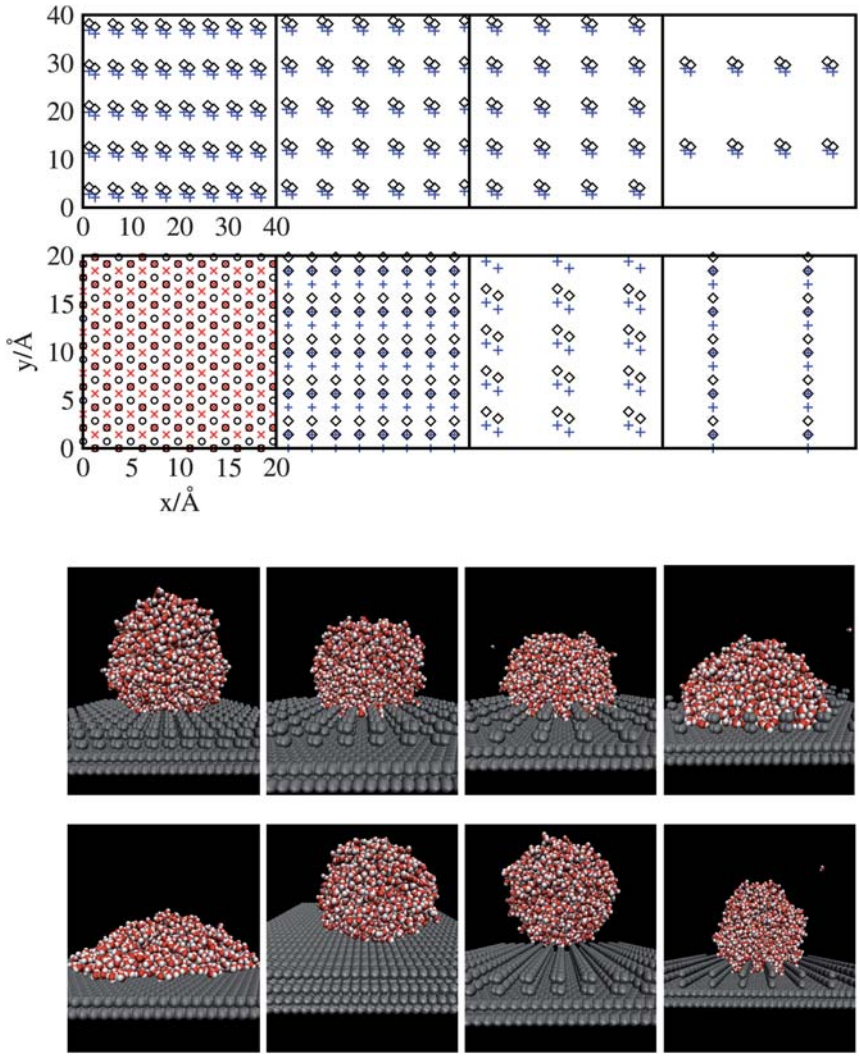

Fig. 1 *Top*: Simplified representation of surface topologies under study. Lower row, L to R: 2-layer (111) surface with no asperities, 1/2 coverage by asperities, 1/6 coverage, 1/8 coverage with rows of asperities along the *y*-axis. Upper row, L to R (note different scale): 1/8 coverage, 1/12 coverage, 1/16 coverage, 1/32 coverage. Red ×'s represent the first layer, black circles the second, black diamonds the third, blue +'s the fourth layer. The first two layers are shown only for the regular (111) surface. *Bottom*: Simulation snapshots of sessile water drops, on the same surfaces as in the top part of the figure. All snapshots except the 1/6 coverage surface, which is hydrophobic (Row 2 of Table 1) are for hydrophilic surface atoms (Row 1 of Table 1).

As the surface coverage is reduced below $\approx$ 10%, we observe that the contact angles begin to lower. The reason for this lowering is that, when the spacing between asperities reaches $\approx$ 10 Å, *i.e.* the size of a few water molecules, some of the water molecules can start to penetrate into the top two layers. This contact angle dependence on the asperity coverage, f_a, on a hydrophobic substrate (top curve in Fig. 2) is qualitatively identical to the experimental dependence on PF_3-coated silicon surface covered by $\sim$5 μm wide, cylindrical asperities, plotted as a function of spacing factor $S_f = 2\pi^{-1/2} f_a^{1/2}$ (Fig. 3a of Bhushan and coworkers in Ref. 28). The abrupt decline in the contact angle at low coverage is similar to that expected

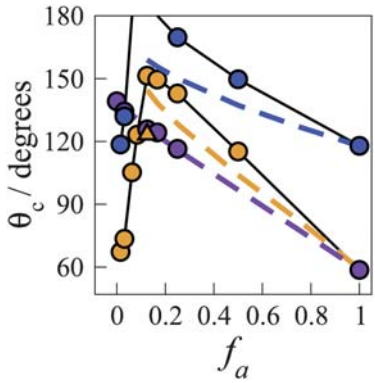

Fig. 2 Contact angles as a function of the surface coverage, f_a, by the asperities, determined from several 400 ps MD simulations (4 × 400 ps for smooth surfaces, up to 12 × 400 ps near the threshold for water penetration). Orange circles: surfaces with the hydrophilic potential, contact angle on a smooth surface, θ_1, equal to 59°; Orange triangle: the surface constructed with rows of asperities along the *y*-axis; Blue circles: surfaces with hydrophobic potential, $\theta_1 = 118°$; Purple circles: mixed surfaces with hydrophobic (2) and hydrophilic (1) components with characteristic contact angles on smooth surfaces of each component $\theta_1 = 59°$, $\theta_2 = 139°$. Solid lines: guide to the eye. Dashed lines: predictions from the Cassie–Baxter equation, in respective colors. Error bars (one standard deviation in the mean) are not shown since they are typically smaller than the symbol size.

upon transition to the Wenzel regime, however, our observed contact angles are never reduced below those observed on the smooth surfaces, in contradiction of the Wenzel equation prediction for hydrophilic substrates. As the surface coverage approaches zero, θ_c gradually returns to the values observed on atomically smooth surfaces.

Comparing the results at the two different patterns of 1/8 coverages (see Fig. 1) demonstrates the effect that different surface topologies can have on the observed contact angles. Here, the fact that one of the surfaces allows water penetration (orange triangle in Fig. 2), while the other does not, causes a difference in the contact angle of about 25°.

Our finding that the Cassie–Baxter equation provides a good description of the contact angle dependence on the smooth but chemically heterogeneous surface agrees with the related modeling studies[14,15,29] where as long as the size of the different domains was well below the size of the drop, the Cassie–Baxter equation was found to hold true. Deviations from the Cassie–Baxter prediction for the rough surfaces are more difficult to explain. One possibility is that there could be kinetic effects, which cause the drop to remain in a metastable state with an increased contact angle, without being able to cross the kinetic barrier to the state where quantitatively Cassie–Baxter behavior would manifest. On macroscopically rough hydrophilic surfaces, a metastable Cassie–Baxter regime has been predicted[30] and demonstrated experimentally[31] for special geometry of the asperities. In the present study, for nanodroplets on a macroscopically smooth surface with nanoscale asperities, especially near the threshold for water penetration, it did take up to 1 ns for the contact angles to slowly lower until they stabilized at their final values. Therefore if a kinetic barrier is the cause for the deviation from the Cassie–Baxter predictions, it must have a timescale much greater than 1 ns, which seems less likely for the small nanodroplets considered. Further, explaining the deviation from Cassie–Baxter behavior in terms of contact angle hysteresis would not conform with the observation that hysteresis primarily occurs on hydrophilic surfaces, and not hydrophobic ones.[14]

Another factor that could contribute to the increase in contact angles on both types of corrugated surfaces is relatively weak attraction of water molecules to

nanoscale asperities. When the roughness occurs on the length-scale comparable to the range of attractive forces between the substrate and water molecules, the attraction of water molecules to an asperity is appreciably weaker than the attraction to an equally distant extended surface.

A major reason why we never see the Wenzel state would appear to be the very shallow depth of our rough surfaces. This is consistent with a DFT-based analytical study which demonstrated that the Wenzel state cannot be produced when the surface roughness is very shallow.[17] Indeed, contact angles agreeing with the Wenzel prediction have been produced by another MD study where the depth of the surfaces was much more pronounced than ours.[15] However, we note that when the depth of the roughness is close to the dimensions of the water drop, the location of the drop/substrate contact plane becomes ambiguous.

Interfacial hydrogen bonding

The number of interfacial hydrogen bonds has a direct impact on the interfacial free energy of the water–surface interface, which in turn affects the contact angles *via* Young's equation, $\cos\theta_c = (\gamma_{sv} - \gamma_{sl})/\gamma_{lv}$. We have computed the average number of hydrogen bonds for interfacial water molecules and plot these as a function of the surface fraction of the partial surface layers in Fig. 3. Two water molecules are presumed to share a hydrogen bond when oxygen–oxygen distance $r_{OO} < 3.5$ Å, the distance $r_{OH} < 2.45$ Å, and the angle between the r_{OO} and r_{OH} vectors is $< 30°$.[32] One of the waters participating in the bond must be within σ_{CO} of one of the surface "carbons". Fig. 3 shows that as the surface fraction decreases from full coverage, the number of interfacial hydrogen bonds decreases, in agreement with other results showing the same trend as the water–surface interaction becomes more hydrophobic.[33]

However, as the surface coverage lowers towards the threshold for water penetration, the number of interfacial hydrogen bonds rises and reaches a maximum for surface coverage ≈ 0.02 to 0.05. This can be attributed to the fact that at coverages in this range the water molecules may form bonds around the asperities in analogy to

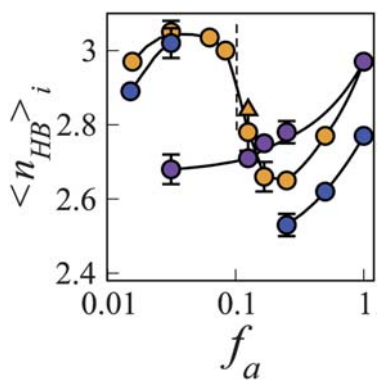

Fig. 3 The number of hydrogen bonds formed by interfacial water molecules as a function of the surface fraction of filled atomic positions in the top two layers of graphite. Interfacial water molecules reside within the range of the repulsive part of the water-surface potential, *i.e.* $< \sigma_{CO}$, from any surface atom. The vertical dashed line roughly indicates where the water molecules can start to penetrate into the partially filled surface layers. The color symbols have the same meaning as in Fig. 2. Black lines are guides to the eye. There are no data for the hydrophobic surface (blue circles) within the interval $0.08 < f_a < 0.25$ since a water drop detaches from the surface in this regime (see the range in Fig. 1 with apparent contact angle exceeding 180°). Indicated error bars are one standard deviation of results from individual 400 ps trajectories (not shown when smaller than the symbol size).

hydration of small solutes,[34,35] hence raising the number of bonds formed above the maximum of three for a planar interface.[36,37]

Droplet translation

Because of thermal fluctuations, the droplets move randomly along the surface, showing quite different mobilities for different substrate types. To quantify these findings, we have determined apparent diffusion constants $D_{x,y}$ in directions parallel to the interface (Fig. 4). Each of these diffusion constants has been derived from mean-square displacements of the drop's center of mass observed in about ten 400 ps trajectories. Despite some statistical uncertainty, they represent useful measures of the mobility of the water drops. We see that the mobility is high in all cases where water molecules cannot penetrate into the partially filled surface layers. However, as the water molecules penetrate the top layers, for the hydrophilic substrate we see that the mobility of the water drops lowers dramatically. In this case, the asperities pin the water drops in essentially one place, at least over the characteristic timescale of our simulation. Remarkably, this pinning is evident even at the lowest coverage we simulated, where only $O(1)$ asperity is located under the water drop. We note also the interesting case where water molecules may freely penetrate only along one lateral axis, due to the presence of a "wall" of surface atoms (the last graph in the top section in Fig. 1). Here the diffusion constant parallel to the rows of aligned asperities remains high, but the drop cannot diffuse across the asperities in the perpendicular direction. If the underlying water–surface interaction is hydrophobic, on the other hand, the presence of the asperities does not have the same impact on the mobility of the water drop. Apparently in this case the water

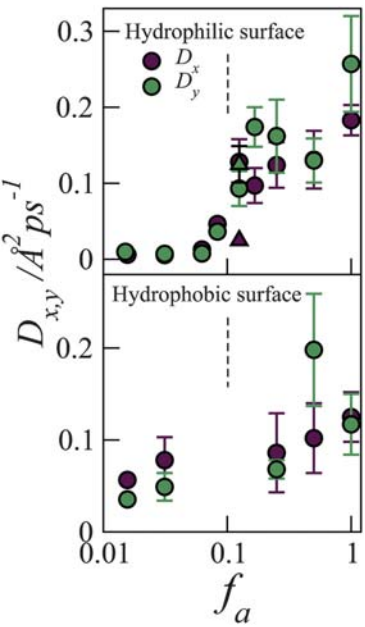

Fig. 4 Apparent diffusion constants $D_{x,y}$ of sessile nanodrops as a function of the surface coverage, f_a, for: Top graph; hydrophilic Lennard-Jones interactions and Bottom graph; hydrophobic Lennard-Jones interactions (first and second row in Table 1). The diffusion constants were determined from the slope of the mean-squared displacement in x and y directions at times between 30 and 40 ps. The triangles represent the surface constructed with rows of asperities along the y-axis. Error bars are one standard deviation in the mean (not shown when smaller than the symbol size.

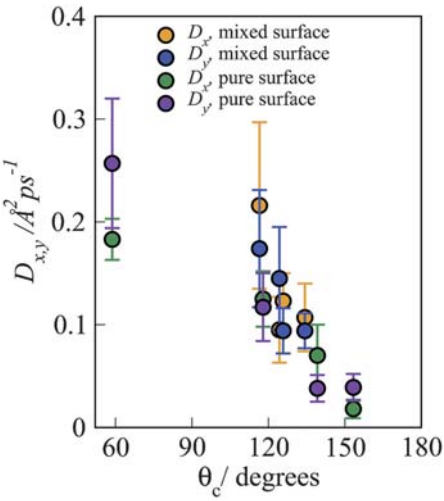

Fig. 5 Diffusion constants $D_{x,y}$ of sessile water drops as a function of the contact angle on a smooth atomic surface. Lennard-Jones parameters for each pure surface's water–carbon interactions are listed in Table 1, while the mixed surface is the same as the purple circles in Fig. 2 and 3. Vertical error bars are one standard deviation in the mean, while the uncertainty in the contact angle is $\pm 1^\circ$.

molecules remain able to flow around the asperities even when they can penetrate into the partially vacant surface layers.

Another interesting finding has to do with the mobility of water drops on an atomically smooth surface without any partial surface layers. These results are shown in Fig. 5. In this case, it appears that the water drops move faster on a hydrophilic surface than a hydrophobic one. For a fluctuation-driven process like the droplet motion on a flat surface, this apparently contradictory result may be explained in terms of stronger surface–water attraction in the case of the hydrophilic surface, which may allow larger random fluctuations in the contour position of the water drop. In the present scenario, thermal fluctuations contribute to the motion of the drop as a whole. Note that thermal motion is the sole cause of the droplet diffusion in our system. If additional forces were at play, *e.g.* due to gravity on a sloping surface or due to wind on a lotus leaf,[9,16,38] the drops would be much more mobile. The effect of surface texture on the droplet mobility under a systematic external force[39] would be different as well.

IV. Conclusions

The majority of prior computational studies of wetting on corrugated surfaces considered mesoscopic length scales, where dynamical issues dominate whether superhydrophobic Cassie–Baxter states or fully wetted Wenzel-like states are observed. For instance, Koishi and coworkers[13] show that if a water drop impacts on a hydrophobic pillared surface with a spacing of 12.3 Å with sufficient velocity, it will overcome an energy barrier between the Cassie–Baxter state and the Wenzel state where it can penetrate between the pillars. What is unique about our study is that we probe very small length scales, where water molecules are prevented from penetrating between asperities by not only energetic or dynamical considerations, but also sterically. Thus, we probe the lowest length scales where a corrugated surface can be completely wetted, regardless of whether the substrate material is hydrophobic or hydrophilic.

We emphasize two new findings pertinent to nanoscale roughness:

First, we demonstrate that roughness on this length scale renders hydrophilic surfaces more hydrophobic, a trend opposite to observations on macroscopically rough materials. Second, we show that a superhydrophobic surface with a contact angle of 180° can also be achieved when surface roughness is limited to the nanoscale alone.

The increase of the apparent contact angle of an intrinsically hydrophobic material ($\theta_c = 118°$) in the presence of surface vacancies qualitatively conforms to, but exceeds the effect predicted by the Cassie–Baxter equation. Upon further decrease in the coverage, the contact angle gradually decreases towards the value characteristic of the original, smooth surface as the water droplet surrounds the asperities.

Our results for the hydrophilic substrate (contact angle of the asperity-free surface below 90°), contradict the prediction of the conventional Wenzel relation according to which the roughness should enhance the surface hydrophilicity. In fact, the qualitative structure of the drop-surface system differs little on either surface; the only difference is that on the hydrophobic surface, an "ultrahydrophobic" state with the maximal contact angle $\theta_c = 180°$ is observed when the surface coverage lies within the window between ~8–25%. Rough interpolation of our results would suggest that this state could be achieved *via* atomic corrugation of surfaces with intrinsic contact angles exceeding 90°, the traditional boundary dividing hydrophilic and hydrophobic surfaces. When the vacancies are replaced by extremely hydrophobic atoms, the behavior predicted by the Cassie–Baxter equation is observed.

The upward deviations from macroscopic predictions of the contact angle can arise from several effects. First we note reduced water/surface attraction when the roughness occurs on the length-scale comparable to the range of intermolecular forces. We hypothesize metastable vapor pockets trapped between hydrophilic asperities can also contribute to the observed contact angle increase although the Wenzel equation suggests a reduction in contact angle if the substrate below the drop is in a fully wetted state. We demonstrate that the reduction in hydrogen bonding represents a major contribution to the increase in surface free energy and the contact angle on the rough surfaces. While complete (100%) surface coverage by the asperities renders surface properties close to those of the original (zero coverage) smooth surface, we observe the maximal contact angle, and minimal hydrogen bonding among interfacial water molecules in the neighborhood of $15 \pm 5\%$ coverage, corresponding to an inter-asperity separation of two or three water molecules.

In contrast to the static contact angle measurements, the dynamics of droplet mobility is much more affected by the corrugations on the hydrophilic substrate compared to the hydrophobic one. The mean squared displacement of the droplet's center of mass (associated with thermal motion and droplet shape fluctuations) as a function of time shows a strong pinning effect by hydrophilic asperities. Lateral diffusion of the droplet as a whole is relatively fast on asperity-free surfaces (and, equivalently, on surfaces with 100% coverage), with the droplet being *more* mobile when the surface is hydrophilic. The droplet mobility is generally reduced in the presence of surface corrugations, however, the effect is much stronger on hydrophilic surfaces, where we observe a dramatic slow down of the droplet translation for asperity coverage as low as 1%. In the case of a nanodrop comprising 2000–4000 water molecules, this coverage corresponds to $O(1)$ asperities under the droplet base. A minute surface decoration proves sufficient to change the droplet mobility by an order of magnitude or more.

Acknowledgements

This work was supported by the National Science Foundation through awards CHE-0718724 (to A.L.) and CBET-0432625 (D.B.). We acknowledge the support by the National Science Foundation through TeraGrid resources (CHE090108). We thank Jim Henderson for pointing out the proper use for Eqs. (1–3).

References

1 R. N. Wenzel, *Ind. Eng. Chem.*, 1936, **28**, 988.
2 A. B. D. Cassie and S. Baxter, *Trans. Faraday Soc.*, 1944, **40**, 546.
3 L. C. Gao and T. J. McCarthy, *Langmuir*, 2009, **25**, 7249.
4 G. McHale, *Langmuir*, 2007, **23**, 8200.
5 L. C. Gao and T. J. McCarthy, *Langmuir*, 2007, **23**, 13243.
6 L. C. Gao and T. J. McCarthy, *Langmuir*, 2007, **23**, 3762.
7 P. S. Swain and R. Lipowsky, *Langmuir*, 1998, **14**, 6772.
8 A. Marmur and E. Bittoun, *Langmuir*, 2009, **25**, 1277.
9 C. Dorrer and J. Ruhe, *Soft Matter*, 2009, **5**, 51.
10 J. Hautman and M. L. Klein, *Phys. Rev. Lett.*, 1991, **67**, 1763.
11 W. Mar, J. Hautman and M. L. Klein, *Comput. Mater. Sci.*, 1995, **3**, 481.
12 B. Widom, Personal communication.
13 T. Koishi, K. Yasuoka, S. Fujikawa, T. Ebisuzaki and X. C. Zeng, *Proc. Natl. Acad. Sci. U. S. A.*, 2009, **106**, 8435.
14 C. Yang, U. Tartaglino and B. N. J. Persson, *Eur. Phys. J. E*, 2008, **25**, 139.
15 M. Lundgren, N. L. Allan and T. Cosgrove, *Langmuir*, 2007, **23**, 1187.
16 G. Carbone and L. Mangialardi, *Eur. Phys. J. E*, 2005, **16**, 67.
17 G. O. Berim and E. Ruckenstein, *J. Chem. Phys.*, 2008, **129**, 014708.
18 H. J. C. Berendsen, J. R. Grigera and T. P. Straatsma, *J. Phys. Chem.*, 1987, **91**, 6269.
19 S. Plimpton, *J. Comput. Phys.*, 1995, **117**, 1.
20 C. D. Daub, D. Bratko, K. Leung and A. Luzar, *J. Phys. Chem. C*, 2007, **111**, 505.
21 T. Werder, J. H. Walther, R. L. Jaffe, T. Halicioglu and P. Koumoutsakos, *J. Phys. Chem. B*, 2003, **107**, 1345.
22 R. L. Jaffe, P. Gonnet, T. Werder, J. H. Walther and P. Koumoutsakos, *Mol. Simul.*, 2004, **30**, 205.
23 D. Bratko, C. D. Daub and A. Luzar, *Phys. Chem. Chem. Phys.*, 2008, **10**, 6807.
24 D. Bratko, C. D. Daub and A. Luzar, *Faraday Discuss.*, 2009, **141**, 55.
25 D. Bratko, R. A. Curtis, H. W. Blanch and J. M. Prausnitz, *J. Chem. Phys.*, 2001, **115**, 3873.
26 D. Bratko, C. D. Daub, K. Leung and A. Luzar, *J. Am. Chem. Soc.*, 2007, **129**, 2504.
27 M. Nosonovsky; B. Bhushan In *12th International Conference on Vibrations at Surfaces Erice*, ITALY, 2007; Vol. 20.
28 B. Bhushan, M. Nosonovsky and Y. C. Jung, *J. R. Soc. Interface*, 2007, **4**, 643.
29 J. Wang, D. Bratko and A. Luzar, Manuscript in preparation, 2010.
30 J. Wang and D. Chen, *Langmuir*, 2008, **24**, 10174.
31 J. Wang, F. Liu, H. Chen and D. Chen, *Appl. Phys. Lett.*, 2009, **95**, 084104.
32 A. Luzar, *J. Chem. Phys.*, 2000, **113**, 10663.
33 C. Y. Lee, J. A. McCammon and P. J. Rossky, *J. Chem. Phys.*, 1984, **80**, 4448.
34 F. H. Stillinger, *J. Solution Chem.*, 1973, **2**, 141.
35 D. Chandler, *Nature*, 2005, **437**, 640.
36 A. Luzar, S. Svetina and B. Zeks, *Chem. Phys. Lett.*, 1983, **96**, 485.
37 A. Luzar, S. Svetina and B. Zeks, *J. Chem. Phys.*, 1985, **82**, 5146.
38 D. Quere, *Rep. Prog. Phys.*, 2005, **68**, 2495.
39 J. D. Halverson, C. Maldarelli, A. Couzis and J. Koplik, *J. Chem. Phys.*, 2008, **129**, 164708.